



## Impact of monsoon transitions on the physical and optical properties of aerosols

C. E. Corrigan,<sup>1</sup> V. Ramanathan,<sup>1</sup> and J. J. Schauer<sup>2</sup>

Received 14 June 2005; revised 23 March 2006; accepted 13 June 2006; published 27 September 2006.

[1] Project Atmospheric Brown Cloud (ABC-Asia) has focused on measuring the anthropogenic influence of aerosols, including black carbon, to determine the extent of sunlight dimming and radiative forcing over the Asian region. As part of this project, an observatory was built in the Republic of Maldives for the long-term monitoring of climate. An inaugural campaign was conducted to investigate the influence of the shifting monsoon seasons on aerosols and climate change. The presence of black carbon and other anthropogenic aerosols over the Indian Ocean varies with the cyclic nature of the Indian Monsoon. Roughly every 6 months, the winds change directions from southwest to northeast or vice versa. From June to October the wet monsoon brings clean air into the region from the Southern Hemisphere. Conversely, the dry monsoon brings polluted air from the Indian subcontinent and Southeast Asia from November through April. As a result, the region becomes charged with black carbon and other anthropogenic pollutants during the dry monsoon. In 2004 the transition between the clean and polluted seasons resulted in nearly an order of magnitude increase of scattering and absorbing aerosols. The change was foreshadowed with small events over a 1 month period prior to the abrupt arrival of pollution over a period of a few days as air from India and Southeast Asia arrived in the Maldives at the surface level. The new, polluted aerosol was characteristically darker since the black carbon concentration increased more substantially than the overall aerosol scattering. As a result, the aerosol coalbedo at a wavelength of 550 nm showed an increase from an average of 0.028 to 0.07. Black carbon mass concentrations increased by an order of magnitude from 0.03 to 0.47  $\mu\text{g}/\text{m}^3$ . These measurements suggest a large increase in the aerosol radiative forcing of the region with the arrival of the dry monsoon.

**Citation:** Corrigan, C. E., V. Ramanathan, and J. J. Schauer (2006), Impact of monsoon transitions on the physical and optical properties of aerosols, *J. Geophys. Res.*, *111*, D18208, doi:10.1029/2005JD006370.

### 1. Introduction

[2] Over the past decade, global attention has focused closely on issues of climate change due to human activity. Primary concern has focused on the emission of greenhouse gases as a byproduct of energy production using fossil fuels and the effect these gases have on the solar radiation budget. The role of greenhouse gases in global climate change is complicated by the contribution of additional factors, such as the presence of natural and anthropogenic atmospheric particulate matter.

[3] Atmospheric particulates, or aerosols, affect the climate by altering the solar radiation balance through several mechanisms, primarily light scattering, light absorption, and cloud modification [*Intergovernmental Panel on Climate Change*, 2001]. Accurate measurements of aerosol physical and optical properties are important for correctly determin-

ing the radiative forcing over a region. Aerosols influence incoming and outgoing radiation both directly and indirectly. Direct effect parameters are principally concerned with light scattering and light absorption. Scattering and absorption are both influenced by the particle size, hygroscopic growth, and concentration. Light absorption by particulate matter is also highly dependent upon the particle composition. The primary component affecting aerosol light absorption is black carbon (BC) since it is efficient at absorbing light at all wavelengths. Black carbon is a byproduct of incomplete combustion and is a constituent of soot. The importance of black carbon as a factor in regional climate change has been demonstrated in numerous modeling studies [*Ramanathan et al.*, 2001; *Chung et al.*, 2002; *Menon et al.*, 2002; *Jacobson*, 2002; *Ramanathan et al.*, 2005]. During the INDOEX (Indian Ocean Experiment) campaign, BC proved to dominate the radiative forcing over the Indian Ocean during the winter season [*Ramanathan et al.*, 2001] and manifested itself as a persistent brown cloud (or haze) that was observed throughout the region.

[4] The INDOEX campaign was mainly focused on an intensive campaign period and was not intended to produce long-term data. The Atmospheric Brown Cloud Asia project

<sup>1</sup>Scripps Institution of Oceanography, La Jolla, California, USA.

<sup>2</sup>Department of Civil and Environmental Engineering, University of Wisconsin-Madison, Madison, Wisconsin, USA.

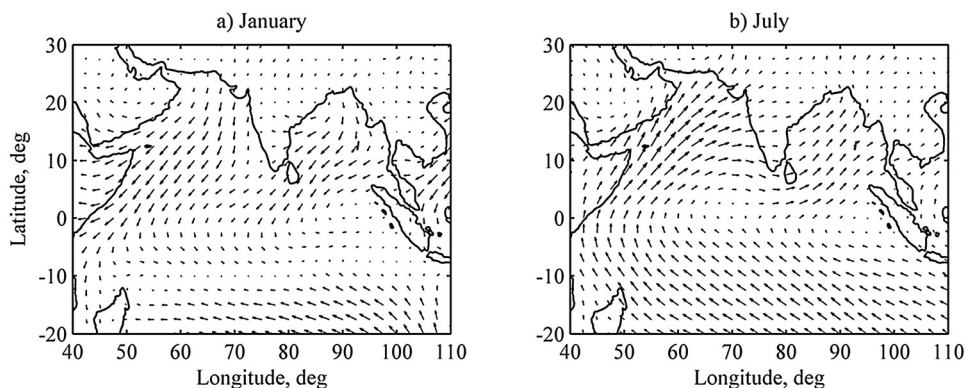


**Figure 1.** Average wind flow patterns over the Indian Ocean during the two monsoon seasons. (a) January, which represents middle of the dry monsoon season; (b) July, which represents the middle of the wet monsoon season.

(ABC-Asia) was designed to pick up where the INDOEX project left off and was intended to provide continuous monitoring of atmospheric pollution, radiative effects and climate change in the Asian-Pacific region [Ramanathan and Crutzen, 2003]. A string of observatories that collect core aerosol and radiation measurements have been deployed or are in the process of being deployed throughout south and east Asia. The first of these stations was the Maldives Climate Observatory-Hanimaadhoo (MCOH) which is located in the Republic of Maldives. The observatory consists of a fully modern facility that operates a broad range of continuous measurements of aerosol physical and optical properties, aerosol chemistry, radiation, and meteorological parameters.

[5] Much of the data discussed in this paper was obtained during the APMEX (ABC Post-Monsoon Experiment) campaign. The start of APMEX coincided with the inauguration of the MCOH facility on 1 October 2004 and the campaign ran for 5 weeks until 7 November 2004. The timing of the campaign was designed to capture the transition between the summer (wet) and winter (dry) monsoon. APMEX consisted of combined aircraft and ground observations in conjunction with a capacity building course for young scientists from the South Asian region. Aerosol and radiation measurements were collected through the entire campaign and a set of core instruments, discussed in a later section, continue to operate permanently at the site.

## 2. Aerosol Observations

### 2.1. Location

[6] The Maldives Climate Observatory at Hanimaadhoo (MCOH) is located at  $6.776^{\circ}\text{N}$  latitude and  $73.183^{\circ}\text{E}$  longitude on the northern point of the island of Hanimaadhoo in the Republic of the Maldives. The Republic of the Maldives is an archipelago of nearly 2000 coral atolls that lie in the Indian Ocean between 200 and 1200 km southwest of the tip of the Indian Subcontinent. The topographies of the islands are quite flat with no natural point in the chain rising above 3 m. As a result, the islands exert very little influence on the oceanic meteorology and therefore serve as superior locations for sampling air coming either from Asia or up from the Southern hemisphere.

[7] The island of Hanimaadhoo is located in the upper northeast corner of the Maldivian archipelago. The island

itself measures approximately 4 km north to south and 1 km east to west. The island is ideally located for sampling air coming from the Indian subcontinent since few influences exist between the sampling site and the mainland. Similarly, only the Maldives archipelago itself and a few distant remote islands influence measurements when air comes from the south.

### 2.2. Monsoon Wind Patterns

[8] A particular advantage of the Maldives location can be attributed to its location downwind of the Indian subcontinent during roughly half of the year. The weather of the geographical region is governed by the same forces that create the Indian Monsoon, which is driven by large-scale circulation patterns that encompass both the Northern and Southern Hemispheres. These patterns change directions on an annual cycle as incoming solar radiation predominately warms different hemispheres. Interhemispheric transport across the intertropical convergence zone results in air being exchanged between the two hemispheres along with any pollution contained within the air mass. In depth details of the monsoon system and pollution transport are described elsewhere [Holton, 1992; Krishnamurti et al., 1998; Verver et al., 2001].

[9] The prevailing wind patterns switch directions with the annual monsoon cycle. In the Maldives, the dry monsoon (often called the Northeast monsoon) is typically active from November to April. Wind generally comes from the northeast and brings air from the Asian continent out over the Indian Ocean. Conversely, from June to September the prevailing winds blow in the opposite direction (from the southwest) and bring warm, moisture laden air up to the Asian continent. These conditions are the wet monsoons (often called the Southwest monsoon) that provide India with most of its annual rainfall. The months of October and May are typically transitional months when the wind patterns are changing directions and tend to be very chaotic.

[10] Figures 1a and 1b illustrate the general wind vectors for the middle of the dry and wet monsoon. The patterns are very distinct with Figure 1a clearly showing the air flow moving off of India to the south and west. As a result, the pollution generated by India and other parts of southern Asia is swept out over the Arabian Sea and the Maldives. Figure 1b shows that the wet monsoon wind patterns carry tropical,

**Table 1.** Instrumentation Operating at ABC Maldives Climate Observatory in Hanimaadhoo<sup>a</sup>

Instrument	Manufacturer	Model
Total particle counter (0.008 – 5 $\mu\text{m}$ ) <sup>a</sup>	TSI	CPC 3022A
Fine particle sizer (0.010 – 0.5 $\mu\text{m}$ ) <sup>a</sup>	TSI	SMPS 3936
Coarse particle sizer (0.5 – 20 $\mu\text{m}$ ) <sup>a</sup>	TSI	APS 3321
Nephelometer (450, 550, 700 nm) <sup>a</sup>	TSI	3563
Absorption photometer: “Aethalometer” (370,430,470,520,590,700,880 nm) <sup>a</sup>	Magee Scientific	AE-31
Meteorological <sup>a</sup>	RM Young	various
Nephelometer, 525 nm (wet)	Ecotech	M9003
Nephelometer, 525 nm (dry)	Ecotech	M9003
Cloud Condensation Nuclei	DMT	CCN Counter
Aerosol mass (PM10, PM2.5): Teflon filter <sup>a</sup>	URG	
EC/OC mass (PM10, PM2.5): Quartz filter <sup>a</sup>	URG	
Inorganic ions (PM10, PM2.5): Teflon filter	URG	
Dust (TSP): Cellulose filter	U. of Miami	
AOTOFMS <sup>b</sup>	UCSD	
Cavity ring down extinction cell*	NASA	
AOD: Handheld <sup>a</sup>	Microtops	II
AOD: CIMEL automated <sup>a</sup>	NASA	

<sup>a</sup>Instruments discussed in this paper.

<sup>b</sup>Present during intensive campaign only.

oceanic air over India which leads to rainfall. This annual cycling of the wind patterns allows for a broad dynamic range of aerosol measurements to be performed in the Maldives. During the summer months (May to September), more pristine air from the Southern Hemisphere can be sampled. Conversely, polluted air from Asia can be measured at the site during the winter months (November to March). The transition from the polluted dry monsoon to the cleaner wet monsoon was recently observed and is reported by *Moorthy et al.* [2005]. Measurements in this paper focus on the transition from the wet monsoon to the dry monsoon and will be categorized according to the sampling periods of pretransition (wet monsoon), transitional, and posttransition (dry monsoon).

### 2.3. Instrumentation

[11] Table 1 provides a complete accounting of the aerosol instrumentation present at the MCOH site. The data reported in this paper are from the following instrumentation. A condensation nuclei counter (TSI CPC Model 3022) measured total particle concentrations in the size range between 0.008  $\mu\text{m}$  and 5  $\mu\text{m}$  diameter. Size distributions were measured by two separate instruments. A scanning mobility particle sizer (TSI SMPS Model 3936) detected particles between 0.01  $\mu\text{m}$  to 0.5  $\mu\text{m}$  diameter. Additionally, an aerodynamic particle sizer (TSI APS Model 3321) measured particles with diameters between 0.5  $\mu\text{m}$  to 20  $\mu\text{m}$ , which actually was limited by the 10  $\mu\text{m}$  size cut of the inlet system. Contributions from particle sizes greater than 8  $\mu\text{m}$  diameter were underreported, with 8  $\mu\text{m}$  and 12  $\mu\text{m}$  diameter particles estimated to penetrate the system at 95% and 5% efficiency, respectively. A nephelometer (TSI Model 3563) was used to measure total and hemispherical back scattering at three visible wavelengths (450, 550, 700 nm). The absorption coefficient was determined using a filter absorption photometer (Magee Aethalometer Model AE-31), which also was used to make estimates of the black carbon mass concentration. The absorption coefficient was measured at seven wavelengths, 370, 430, 470, 520, 590, 700, and 880 nm. A set of meteorological instruments (RM Young)

measured relative humidity, pressure, temperature, rain gauge, wind speed and wind direction.

[12] Filters provided 24 hour integrated direct measurements of elemental carbon mass, organic carbon mass and total aerosol mass. In addition, filters were used for collection of inorganic ions, tracers for source emissions, and dust content. The filter samplers were set atop the 15 m tower and did not draw from the main pipe, but instead sampled directly from the ambient air. Total aerosol mass concentration was determined by weighing the exposed Teflon filters. The filters were weighed in a temperature and humidity controlled weighing room after equilibrating at  $21 \pm 2^\circ\text{C}$  and  $35 \pm 5\%$  RH for 24 hours using a microbalance that was calibrated with NIST certified weighing standards. Elemental carbon and organic carbon mass concentrations were analyzed by a thermal optical method [*Schauer et al.*, 2003].

[13] The station hosted many additional aerosol and radiation instruments, but the data from these are not covered in this paper. Additional aerosol instruments that are continuously at the observatory include a pair of single wavelength nephelometers (Ecotech Model M9003) employed to sample the total scattering at 525 nm under both ambient and dry relative humidities, and a cloud condensation nuclei counter (DMT CCNC). An Aerosol Time of Flight Mass Spectrometer (AOTOFMS) was operated by UCSD and was present only for the intensive APMEX campaign (7 October to 7 November). Similarly, the NASA operated cavity ring down (CRD) extinction cell was present only for the APMEX campaign.

[14] The nephelometers and CNC counter data consisted of 1 minute averaged values. The aethalometer data, SMPS, and APS data was generated every 5 min. All filter data consisted of 24 hour integrated samples since the filters were changed once per day at 0700 local time. The meteorological data was recorded every 10 seconds.

### 2.4. Sampling Inlet

[15] The laboratory is located 1.5 m above sea level and is surrounded by ocean within 100 m on three sides. The site includes a 15 m tower that rises above the local vegetation to

allow unobstructed solar radiation measurements and aerosol sampling. Aerosol sampling can take place atop a 15 m tower, as with filter sampling, or via a 15 m inlet pipe that carries air down and into the laboratory. The stainless steel main sampling pipe is 20 cm in diameter and is capped with a rain cap/impactor assembly. The impactor is a collection of 15 orifice jets that serve to remove large particles from the sampled air ( $D_{50} = 10 \mu\text{m}$ , or the particle diameter at which 50% of particles were removed was  $10 \mu\text{m}$ .) Airflow through the main pipe was 300 L/min, which maintained laminar flow conditions. Once the main pipe entered the laboratory, only the center air stream was collected via a concentric 15 cm anodized aluminum pipe. This approach minimized wall losses during the long passage through the 15 m sampling pipe, which took more than one minute. The outer sheath air that had been exposed to the outer wall of the main pipe was used as make-up air and could be conditioned to serve as a source of dilution and drying air. The center air from the main pipe was then split into two lines for easier distribution to sampling systems and instrumentation.

[16] The inlet system sampled particles with diameters in the range of 0.01 to  $10 \mu\text{m}$ . Losses due to gravitational settling and inertial impaction were calculated for the entire inlet system using theoretical equations [Baron and Willeke, 2001]. Since the inlet system incorporates a PM10 size cut (Particulate Matter of  $10 \mu\text{m}$  or less are only sampled.), the collection efficiency of the inlet system was designed to be better than 90% for particles with an aerodynamic diameter of  $10 \mu\text{m}$  and better than 98% for particles with a diameter less than  $5 \mu\text{m}$ . The PM10 impactor located at the entrance of the inlet pipe had a 50% cut point for  $10 \mu\text{m}$  particles. Estimated losses based on calculations for  $9 \mu\text{m}$  and  $11 \mu\text{m}$  diameter particles are <10% and >90%, respectively.

[17] The tropical environment in the Maldives provided a challenge for sampling aerosols due to the high relative humidity and water vapor density caused by the warm marine climate. The relative humidity typically ranged from 60% to 90% and was often as high as 95% when rain systems were moving through the region. Temperatures ranged from 25 to  $35^\circ\text{C}$ . Since the laboratory was air conditioned, the instrumentation was housed in a separate room that was maintained at ambient temperatures ( $\pm 1^\circ\text{C}$ ) in order to prevent the condensation of water inside the sampling lines or the instruments due to cooling. As a result, the instruments were able to measure at the approximate temperature and relative humidity of the ambient environment. Internal heat within instruments due to electronics and light sources, such as in the nephelometer, served to artificially raise the temperature in the actual measurement cells and biased the relative humidity at the point of measurement. The nephelometer had an internal temperature that was elevated about  $3^\circ\text{--}4^\circ\text{C}$  over the ambient due to its light source. Consequently, its internal RH sensor would typically read 10% lower than ambient measurements. This phenomenon is a characteristic of all TSI nephelometers regardless of location. Other instruments (described in detail in section 2.4) were also sampling at a biased relative humidity due to internal heat. The aethalometer maintained an internal temperature of around  $2^\circ\text{--}3^\circ\text{C}$  above ambient. The APS had a slight temperature increase within its cell, but the magnitude was not determined. The CPC measurements were unaffected by relative humidity and temperature changes. The SMPS was able to make measure-

ments at true ambient conditions since no significant heat sources affect the sampling path within the instrument.

### 3. Results and Discussion

#### 3.1. Data Quality

[18] All instruments were cleaned and calibrated prior to the study. Flow rates were measured and calibrated using a positive displacement bubble flowmeter (Gilibrator, Sensidyne Corp.). The scattering responses of the nephelometers were calibrated using  $\text{CO}_2$  as a span gas and clean, filtered air as the zeroing gas. All nephelometers performed zero checks every 12 hours to correct for any drift in the baseline signals of the photodetectors. The CN counter was calibrated for flow rate and compared to two other CN counters to confirm agreement of total particle concentrations. Because of the high humidity and temperature of the location, the butanol working fluid inside the CN counter needed to be changed every two days. Beyond two days, the butanol would collect too much water from the air and the instrument would eventually fail to detect particles. The SMPS had similar maintenance performed on its CN counter. The APS and aethalometer were also calibrated for sample flow rate.

[19] Data were screened for abnormalities and validated prior to being incorporated into the finalized data sets that were used for analysis. The most common reasons for dismissing data were due to instrument failures and periods of known local contamination, such as construction activities.

[20] The nephelometer data required the application of a correction routine to compensate for truncation errors and nonideality in the geometry of the instrument [Anderson and Ogren, 1998]. The correction factors were derived by utilizing the multiple wavelengths of the nephelometer to derive the angstrom coefficient, which was then applied to a correction algorithm. The nephelometer corrections typically increased the total scattering coefficients by between 20 and 30% over the raw values. The backscattering coefficients were not noticeably affected by the corrections.

[21] The manufacturer of the aethalometer (Magee Scientific) calibrates the instrument to output data on the mass concentration of absorbing material at 7 different wavelengths, although only the 880 nm channel is considered valid by the manufacturer for black carbon mass concentrations. Absorption coefficients ( $\text{m}^{-1}$ ) were calculated from the original data ( $\mu\text{g}/\text{m}^3$ ) using the method outlined below.

[22] The filter absorption method employed in the aethalometer has two known impediments that interfere with accurate measurements [Arnott et al., 2005]. These interferences must be accounted for in order to obtain reliable absorption coefficients and black carbon mass [Sheridan et al., 2005]. First, the deposition of scattering material onto the filter produces a small amount of absorption signal. This interference is most prominent when the scattering is high with respect to the absorption. Secondly, the response of the absorption signal is not linear as the filter darkens due to the collection of BC particles. The absorption deviates from Beer's law due to changes in the multiple scattering paths provided by the quartz filter fibers. Normally, this multiple scattering significantly increases the absorption signal. The embedding of dark particles onto these fibers diminishes the contribution of multiple scattering and renders the method

**Table 2.** Parameters Used by *Arnott et al.*'s [2005] Procedure to Correct the Aethalometer Data

Wavelength, nm	100 $\alpha$	M	$\tau_{a,fx}$
370	1.14	3.467	0.2874
430	1.38	3.569	0.2632
470	1.55	3.629	0.2483
520	1.77	3.695	0.2338
590	2.09	3.770	0.2097
700	2.62	3.849	0.1827
880	3.53	3.875	0.1566

less sensitive to newly deposited dark material. *Arnott et al.* [2005] have recently developed a correction method specifically for the aethalometer. By applying an empirically derived correction routine based on laboratory and field absorption measurements made in conjunction with a photoacoustic photometer, corrected absorption coefficients were extracted from raw aethalometer data. This procedure was employed in this study by applying equation 27 of *Arnott et al.* [2005]. Their equation 27 requires four parameters: SG, 100  $\alpha$ , M and  $\tau_{a,fx}$ , all of which are wavelength-dependent. For SG, the exact values given in Table 1 of *Arnott et al.* [2005] were used. For the parameters M and  $\tau_{a,fx}$  an offset was applied to the values listed in Table 1 of *Arnott et al.* [2005] (see caption for their Table 1). The revised values as used in this study are shown in Table 2. We employ the offset correction factor because the original values given by *Arnott et al.* [2005] were for synthetic laboratory generated aerosols and they found it necessary to apply an offset correction to adapt their values for field measurements. Since the ambient aerosol correction parameters are only given for one wavelength (520 nm), the remaining parameters at the other six wavelengths were estimated by applying the same offset to the best fit line of the laboratory generated parameters. The scattering interference parameter,  $\alpha$ , were adjusted down to about 40% of the original value since the published values produced consistently negative absorption values during clean events. This was partially due to the large proportion of supermicron sea-salt particles. To eliminate the predominance of unrealistic negative absorption coefficients, which only arise from excessive scattering correction, certain clean events (low absorption and normal scattering) were assumed to consist of only nonabsorbing aerosols. As a result, these events were defined as having an absorption coefficient of zero (below detection limits;  $<0.20 \text{ Mm}^{-1}$ ). This brought the scattering correction in agreement with the 2% scattering contribution to absorption that was empirically determined by *Bond et al.* [1999] using the similar particle soot absorption photometer (PSAP).

[23] The uncertainties in the absorption and derived black carbon measurements obtained using aethalometer data come from five main sources.

[24] 1. Instrument noise is significant when trying to retrieve data from short time periods. With longer averaging time periods, the instrument noise becomes extremely small as dark aerosol material builds up on the filter. The manufacturer claims a conservative detection sensitivity of better than 5 ng on the filter. This translates to  $250 \text{ ng/m}^3$  over 5 minutes,  $20 \text{ ng/m}^3$  over 1 hour, and  $<2 \text{ ng/m}^3$  over a 12 hour period. Independent studies have established more practical limits of detection at  $100 \text{ ng/m}^3$  over 1 hour and

$30 \text{ ng/m}^3$  over 3 hours [*Allen et al.*, 1999]. The uncertainty in the flow rate ( $\pm 5\%$ ) becomes the most significant contribution to the instrumental error when working at values 20 times over the detection limit. Flow rate and instrument uncertainties have been propagated through all of the absorption and coalbedo calculations in this manuscript.

[25] 2. Aerosol parameters, such as scattering interference, filter loading, composition, size, etc., systematically bias the filter absorption measurement method. Scattering and filter loading are the primary purpose for utilizing a correction routine. Other aerosol parameters are not well characterized in the literature for their contribution to the overall uncertainty.

[26] 3. Sampling conditions such as rapid relative humidity and temperature changes may have a significant effect on measurements but the influence is minimized if the change occurs gradually or by using long averaging periods.

[27] 4. Another source is uncertainties in method parameters. *Arnott et al.* [2005] does not provide uncertainties for the three parameters that are used in the correction algorithm (see Table 2.) Moreover, the actual value of the parameters is dependent upon aerosol morphology, size, composition, age, etc.; therefore different types of aerosol (fresh, aged, size) require different parameters. While these uncertainties could not be characterized for this manuscript, the large difference seen between the laboratory derived parameters and ambient parameters was recognized. Since any attempt at assigning uncertainties would be arbitrary, errors arising from the correction method were not accounted for in this study. As a result, the provided uncertainties represent only a lower bound for the overall uncertainties in the aethalometer derived data.

[28] 5. Variability in the natural aerosol is undoubtedly the largest contributor to the uncertainty in most of the measurements in this study. Significant changes in aerosol parameters (concentration, size distribution, etc.) routinely occur over the 12 hour (or even seasonal) averaging periods. This variability is shown by calculating the standard deviation of the data over the averaging periods and dominates over the instrument errors in most cases.

[29] As shown later, the estimated uncertainty in the retrieved absorption coefficients ranges from as low as 5% to as large as 40%. These values are shown to be consistent when the aethalometer derived BC mass is compared with a completely independent method using filter based measurements of BC. (section 3.4.)

### 3.2. Aerosol Physical Properties

[30] Aerosol data is continuously collected at the MCOH site, but this work concentrates on the four month period from October 2004 to January 2005. During this time period, the seasonal monsoon pattern undergoes a shift from a southwest source to a northeast source. This transition is also characterized by the rain patterns, with the wet monsoon season ending and the dry monsoon season beginning. As a result, a change in aerosol properties was expected to be observed in conjunction with the large-scale wind change.

[31] Figure 2 visibly captures this transition for the total particle concentration ( $0.008\text{--}5 \mu\text{m}$  diameter). From 10 October to 15 November, the total particle concentration maintained an overall average of  $770 \pm 440 \text{ particles/cm}^3$ . Variability occurred during this time, but the baseline

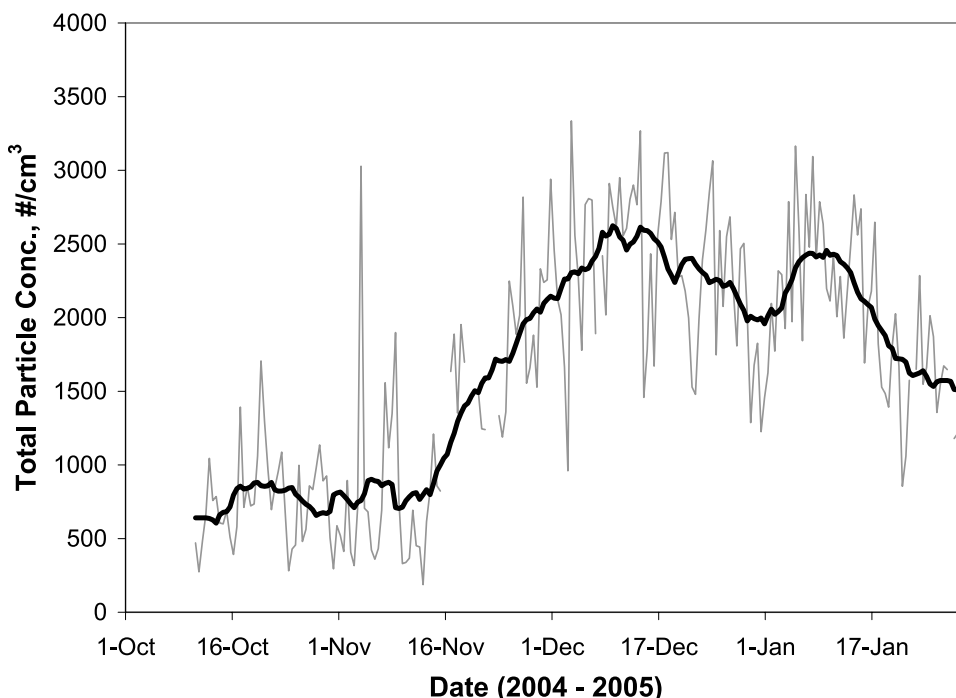


**Figure 2.** Total aerosol concentration ( $0.008 \mu\text{m} > D > 5 \mu\text{m}$ ) at Maldives Climate Observatory at Hanimaadhoo (MCOH) from October 2004 through January 2005.

particle concentration usually returned to a value below 500 particles/cm<sup>3</sup>. A sudden increase in the average baseline particle concentration occurred on 15 November 2004 with particle concentrations increasing by a factor of 3. The average concentration from 15 November to 31 January was  $2100 \pm 560$  particles/cm<sup>3</sup>. This rapid increase in particle concentration marked the arrival of persistent polluted air from the Indian subcontinent. Events prior to 15 November were transient and have been attributed to local particle generation or to sporadic influxes of air from Asia as the monsoon wind patterns were undergoing transition.

[32] To better illustrate the origin of air arriving at the observatory, 6-day wind back trajectories were plotted for selected days during the sampling period using the NOAA Hysplit model [Draxler and Hess, 1998]. Figures 3a, 3b, and 3c show representative back trajectories for the three monsoon conditions that were studied: wet monsoon, transi-

tional, and dry monsoon. The transitional condition referred to the ending of the wet monsoon and the start of the dry monsoon. The back trajectory tracks are for wind arriving at MCOH for 1000 m and below. The similar 100, 200, 300 and 500 m wind trajectories are given as solid black lines and the 1000 m trajectories are given as dashed lines. The sources of elevated pollution levels detected at the observatory on 19 November are readily apparent by looking at the wind back trajectories in Figure 3c. The trajectories passed over southern India just a few days before arriving at the Maldives observatory. Conversely, the relatively pristine air from 15 October appears to have avoided any landmasses and human population centers as seen in Figure 3a. These two examples illustrate the typical sources for both the clean air conditions of the wet monsoon and polluted air conditions during the dry monsoon. Figure 3b shows the more interesting case of mixed air sources. Low-level winds below 500 m

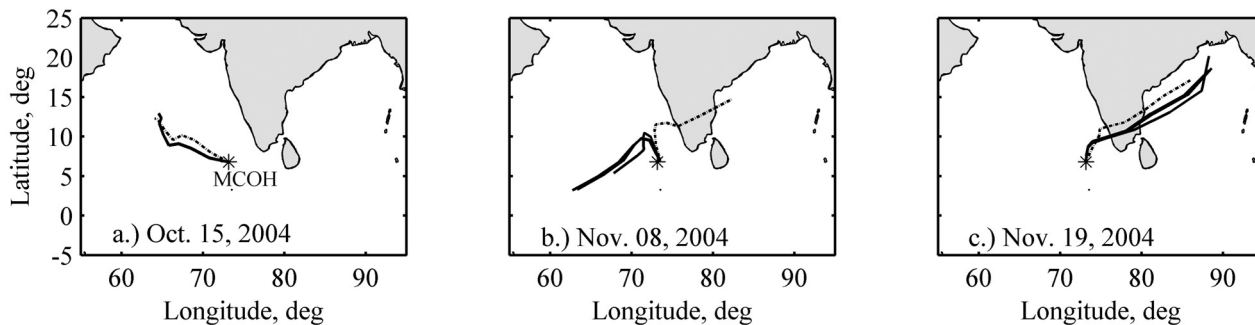


**Figure 3.** Wind back trajectories using the Hysplit model for (a) wet monsoon winds, (b) transitional period, (c) dry monsoon winds. The solid lines are for the 100, 200, 300, and 500 m levels. The dashed line is for the 1000 m level.

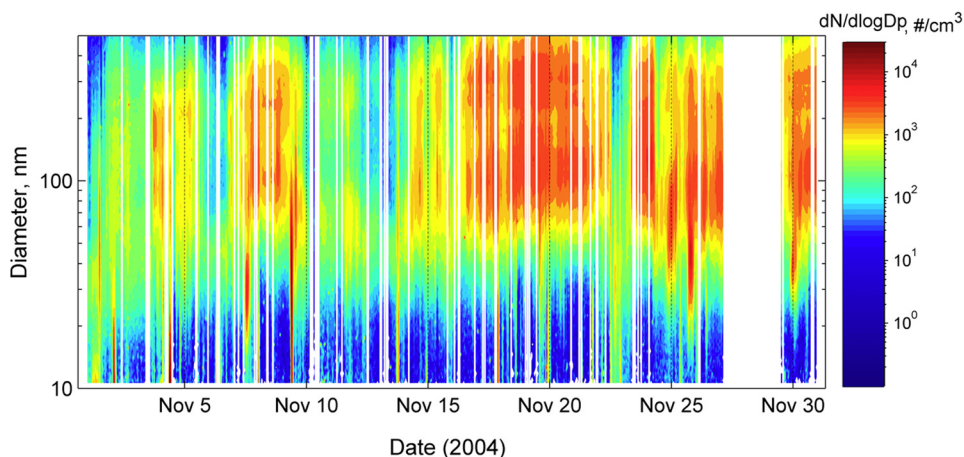


**Figure 4.** Time series of submicron aerosol size distribution collected with a TSI SMPS during the November 2004 at MCOH.

were coming from clean sources in the open ocean to the west of the Maldives, yet winds at 1000 m were originating over southern India. This mixing of wind sources occurred during the transitional period from mid October to mid November and resulted in transient pollution events when upper level air was sporadically carried down to the surface due to small-scale turbulence.

[33] The change in the aerosol particle concentration illustrated in Figure 2 was not simply a uniform increase in concentration across all particle sizes. The proliferation in particles was most dramatic for the submicron size distribution. The size distribution time series for November 2004 shown in Figure 4 was collected with the SMPS and shows that the concentration of accumulation mode particles, loosely defined as particles with a diameter in the range of 100–700 nm ( $100 < D < 700$  nm), significantly increased in mid November, yet particles with a diameter less than 50 nm

showed no noticeable increase in concentration outside of a few isolated events. The lack of small particles indicates an aged aerosol which had sufficient time to coagulate and shift its smaller particles into the accumulation mode. Figure 5 shows representative size distributions from both before and after the monsoon transition (pretransition and posttransition) to illustrate the dramatic change in the aerosol. The unpolluted distributions shown are from 1 and 2 November while the polluted (posttransition) distributions were taken five days after the persistent arrival of polluted air. A large increase occurred for particles with a diameter greater than 50 nm, but very little change occurred for particles below 50 nm.

[34] This substantial change in the submicron aerosol was only partially observed for the supermicron particles. Figure 6 shows selected premonsoon and postmonsoon transition volume size distributions taken from the aerody-

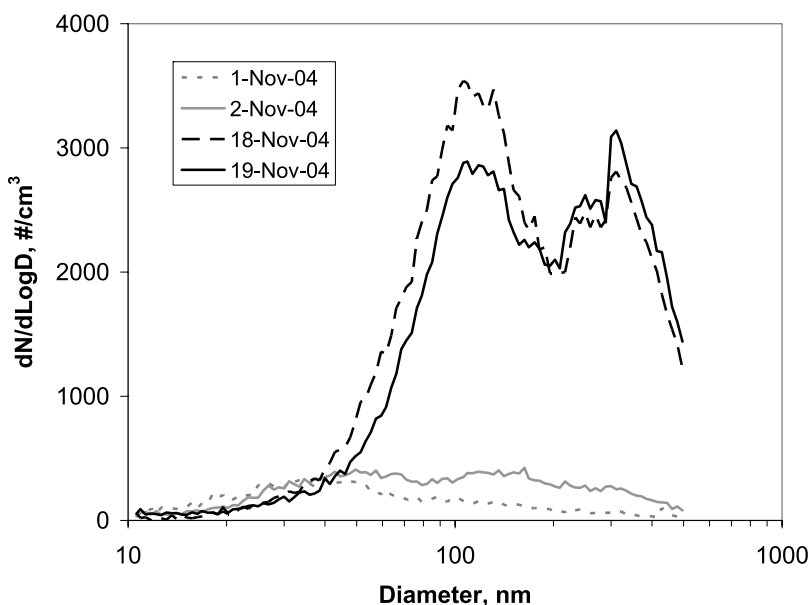


**Figure 5.** Specific examples of averaged aerosol size distributions from the TSI SMPS during the wet monsoon and during the dry monsoon.

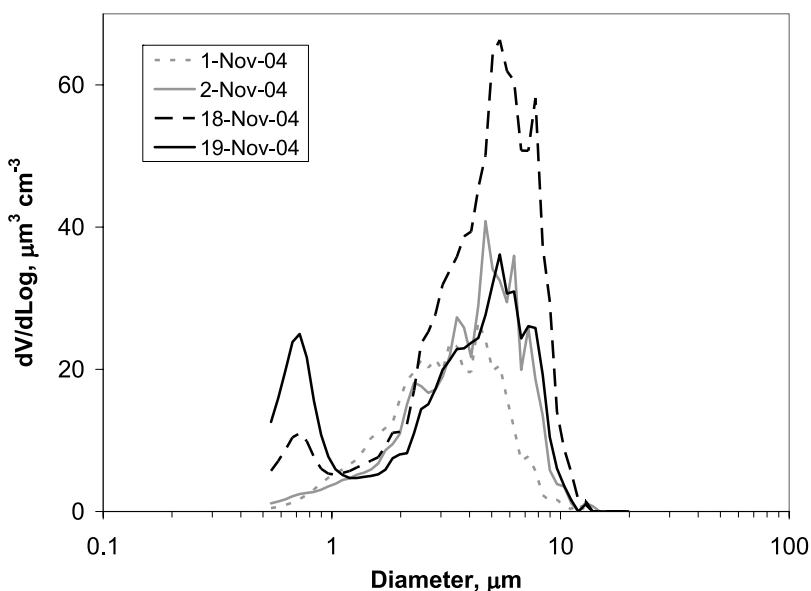


**Figure 6.** Specific examples of averaged supermicron aerosol size distribution from the TSI APS during the wet monsoon and dry monsoon.

namic particle sizer. The dramatic change seen in the submicron aerosol was not as prominent for the supermicron aerosol. An increase in volume was either not observed or was only on the order of 2 or 3 instead of a factor of 10 to 12 as seen during the same time period for submicron aerosol as calculated from the SMPS data. Many of the supermicron aerosol particles originated from the local ocean and surf zone located near the observatory. These areas were a relatively constant source of supermicron aerosols and were most pronounced when the wind came from the north and east due to breaking surf. Supermicron aerosol generated on the Asian mainland was less likely to survive the multiple-

day journey to the observatory since removal processes were more efficient for larger particle sizes. As a result, the increase in the submicron aerosol was much more pronounced than the increase in the supermicron aerosol.

[35] By combining the volume distributions from the APS and the SMPS, total aerosol volume information was obtained. In addition, the total mass of the aerosol was taken directly from mass measurements of Teflon filters collected with a PM10 size cut. Both the calculated aerosol volume derived from the size distributions and the measured filter mass are plotted in Figure 7. The transition on 15 November was also seen in Figure 7, but the change was not as

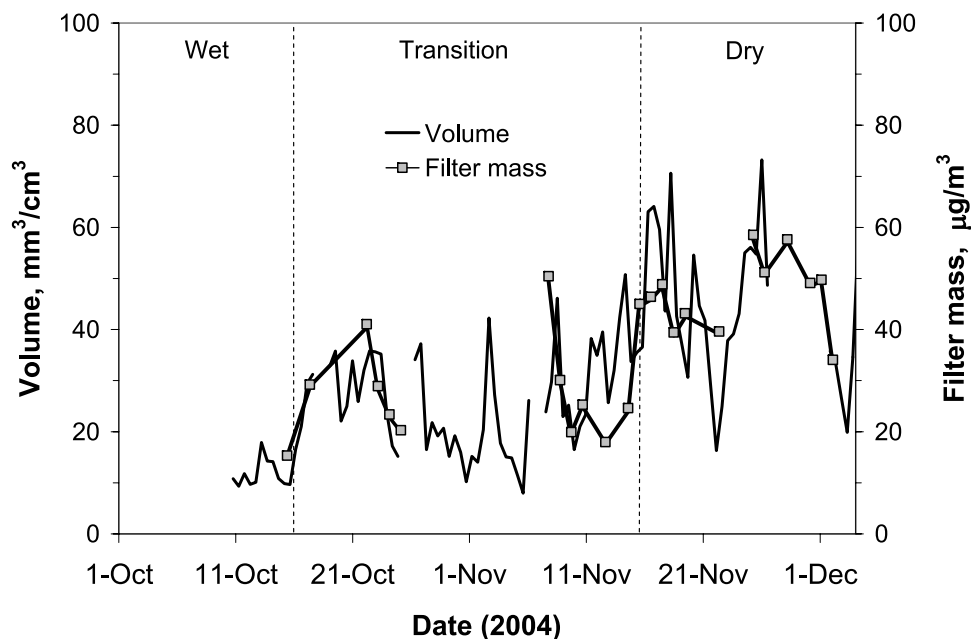


**Figure 7.** Aerosol total mass from filter measurements and total volume taken from SMPS + APS during the monsoon transition.

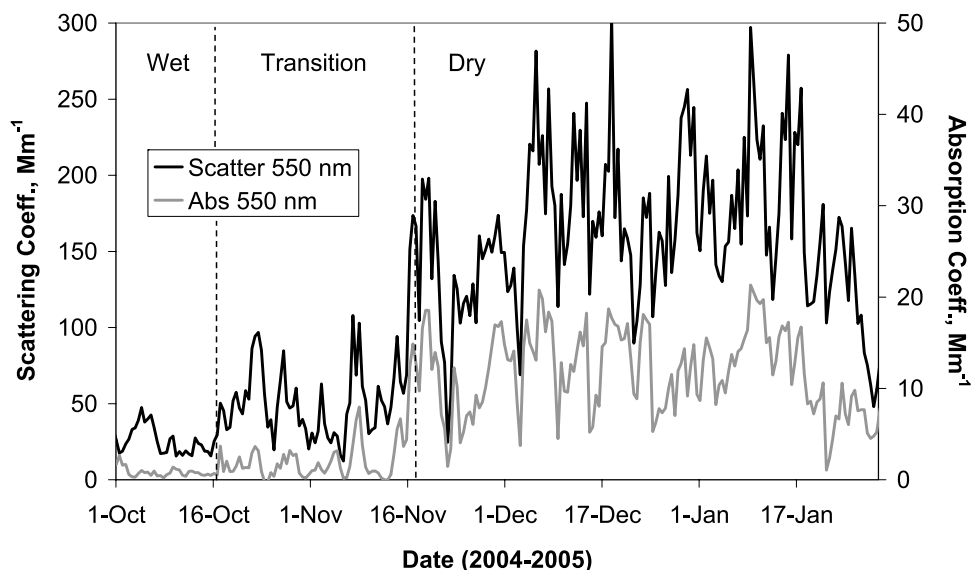


**Figure 8.** Aerosol scattering and absorption coefficients at 550 nm over MCOH.

significant as observed in total particle concentration and submicron aerosol size distribution. This was mostly likely a result of the aerosol volume being dominated by particles coming from local sources, such as supermicron sea salt. These local sources were to some extent consistent during the wet and dry monsoon periods.

[36] The change in the monsoon seasons was apparent in the daily filter mass concentrations. The daily average aerosol mass for PM<sub>10</sub> aerosol was  $18.7 \pm 3.9 \mu\text{g}/\text{m}^3$  prior to 17 October (wet monsoon), was  $28.5 \pm 8.8 \mu\text{g}/\text{m}^3$  for the transition period of 17 October to 15 November (transitional period), and was  $55.1 \pm 14.3 \mu\text{g}/\text{m}^3$  after 15 November (dry monsoon). Similarly, the PM<sub>2.5</sub> cut filters saw an average daily mass of  $8.8 \pm 3.0 \mu\text{g}/\text{m}^3$  for the transitional period and a value of  $19.3 \pm 4.6 \mu\text{g}/\text{m}^3$  after the full arrival of polluted air on November 15th. PM<sub>2.5</sub> filter results prior to 15 October are unavailable. The values for the PM<sub>2.5</sub> mass during the polluted dry monsoon season were similar to the results found by Chowdhury *et al.* [2001], who measured an average PM<sub>2.5</sub> mass concentration of  $17.7 \pm 0.2 \mu\text{g}/\text{m}^3$  during the dry monsoon season as part of the INDOEX campaign.

### 3.3. Aerosol Optical Properties

[37] The monsoon transition is clearly visible in the time evolution of absorption and scattering coefficients at 550 nm as shown in Figure 8. The scattering increased by a factor of 5.6 and the absorption increased by more than a magnitude over the month of November. The scattering averaged  $28.8 \pm 10.8$  (standard deviation of  $1\sigma$ )  $\text{Mm}^{-1}$  during the wet monsoon season in early October and rose to an average value of  $161 \pm 53 \text{Mm}^{-1}$  for the dry monsoon season after the middle of November. Likewise, the absorption coefficient averaged  $0.87 \pm 0.56 \text{Mm}^{-1}$  for early October and climbed to an average of  $11.7 \pm 4.6 \text{Mm}^{-1}$  with the arrival of the dry monsoon. For comparison, previous measurements during the dry monsoon as part of the INDOEX campaign found average scattering coefficients (at 70% RH) and absorption coefficients of approximately 80 and  $20 \text{Mm}^{-1}$ , respectively [Eldering *et al.*, 2002]. The lower scattering values during the

dry monsoon for APMEX were most likely due to the reported INDOEX measurements being for submicron aerosol ( $D < 1 \mu\text{m}$ ) instead of PM<sub>10</sub> ( $D < 10 \mu\text{m}$ ). The difference in the absorption measurements between INDOEX and APMEX can be attributed to natural variability in the aerosol and inconsistencies between absorption measurement methods. The large increase in absorption was a clear indicator that polluted air from the Indian subcontinent had arrived at the Maldives since the only substantial source of broadband absorbing particles is from combustion processes. An increase in scattering might have been attributed to a dust event or sea spray, but probably not at the consistent levels observed after 15 November in the Maldives. Consequently, the scattering increase was also attributed to the arrival of polluted, continental air given the similar increase in the absorption signal.

[38] The scattering and absorption coefficients measured at various wavelengths are presented in Figure 9. The data has been separated into average values for each wavelength during the wet monsoon, dry monsoon, and transitional period. The error bars represent the 95% confidence limit of the average for each monsoon period. The dry monsoon showed a significant increase over the wet monsoon for scattering and an even larger increase for absorption over all wavelengths. For the scattering data in Figure 9a, the angstrom coefficients were 0.50, 0.54, and 1.06 for the wet, transitional, and dry monsoon periods respectively. This reflects the situation illustrated by the size distributions in Figures 5 and 6. The angstrom exponent increased as the supermicron dominated aerosol of the wet monsoon aerosol was overshadowed by additional accumulation mode particles arriving during the dry monsoon. The overall absorption angstrom exponents were 1.38, 1.06, and 0.82 for the wet, transitional, and dry monsoon periods, respectively. Light absorbing organics, biomass smoke, and dust generally produce an enhanced absorption at shorter wavelengths due to the spectroscopic characteristics of chemical bonds. As a result, the presence of light absorbing organics, biomass smoke, and dust produces a larger value for the absorption

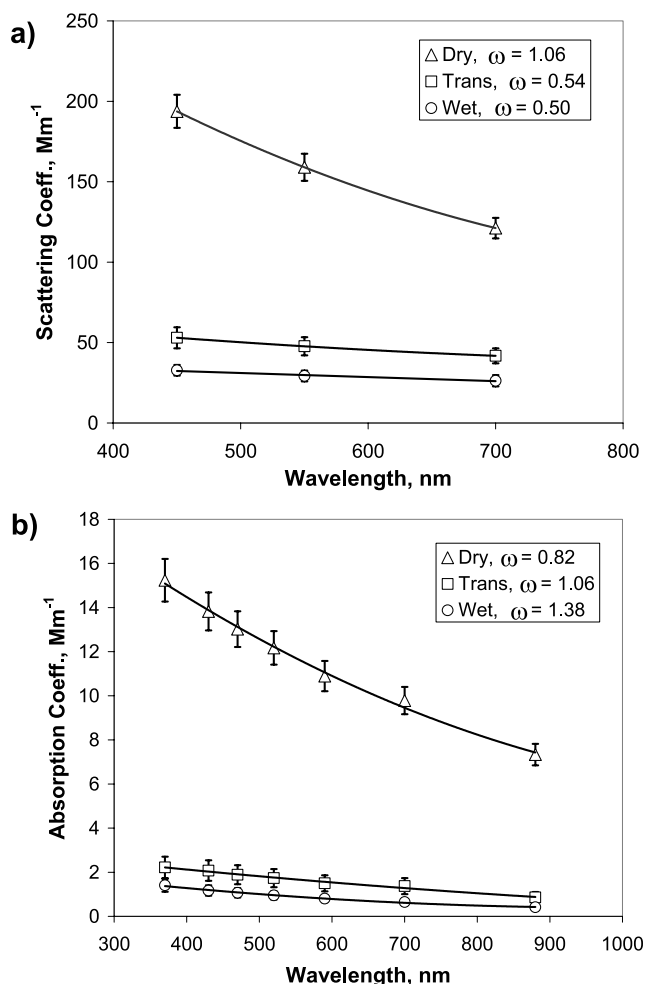


**Figure 9.** Wavelength dependence of the (a) scattering and (b) absorption coefficients and angstrom exponent,  $\omega$ , for each monsoon period. Error bars are 95% confidence limits of the mean values.

angstrom exponent as opposed to pure black carbon, which is a broad band absorber. For example, diesel soot, which has a high component of black carbon, shows much less wavelength dependence than biomass smoke that contains a large portion of light absorbing organic material [Kirchstetter *et al.*, 2004]. The higher proportion of black carbon contained within the aerosol coming from the Asian continent during the dry monsoon is reflected in the significant reduction in the absorption angstrom exponent.

[39] Generally, the polluted air was carried from the Indian subcontinent by winds coming from the north and east. To better illustrate the role of wind direction on variations in the measured aerosol properties, the aerosol absorption data was plotted in conjunction with wind direction information. Figure 10 shows the 12-hour averaged absorption coefficient during the monsoon transition period plotted according to wind direction. Figure 10 focuses on the transitional period between the monsoons. Each of the four directions represents a 90° sector centered on the given direction. The 12-hour average often had winds from other sectors, but only the statistical mode (most common sector) was used to determine the final classification of wind sector. Clearly, the wind from the west was usually quite clean, especially in the wet monsoon (prior to 16 October). Absorption events occurred most often when the wind came from the north and east and briefly exposed the island to continental air. The event on 8 November was an example of this phenomenon. The transition period from 16 October to 15 November) was filled with random and unpredictable wind directions that occasionally carried wisps of polluted air from the mainland. This period represented the transition between the two monsoons. After the onset of the dry monsoon in mid November, the wind direction became more consistent and was primarily from the northeast. Some events during the dry monsoon showed wind coming from the west or south, but the aerosol loading did not significantly decrease (see 21 November and 1–5 December). Even though the wind direction at the observatory suggested that the air was coming from unpolluted regions, back trajectories showed the initial source of the pollution to be the Asian

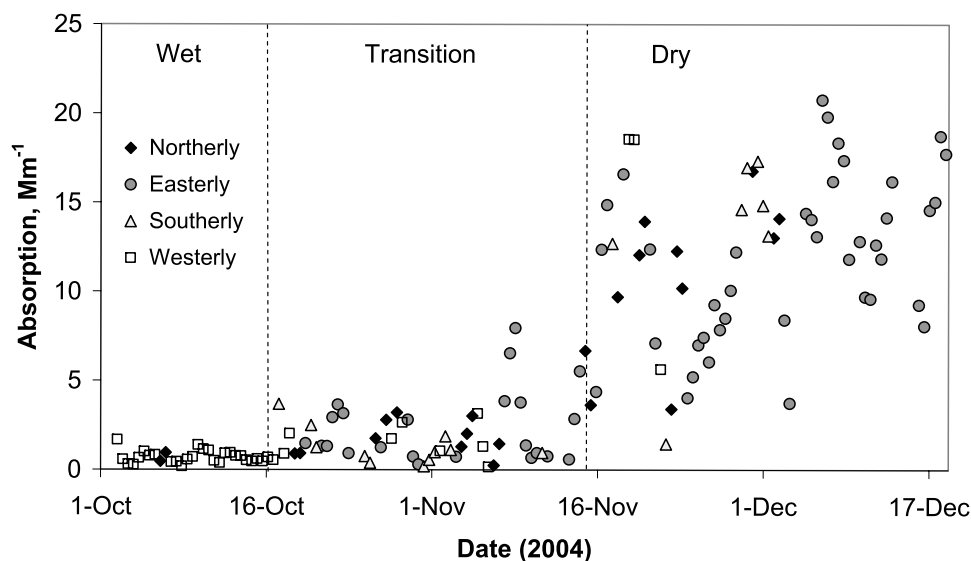


**Figure 10.** Aerosol absorption coefficient at 550 nm over MCOH plotted according to wind direction.

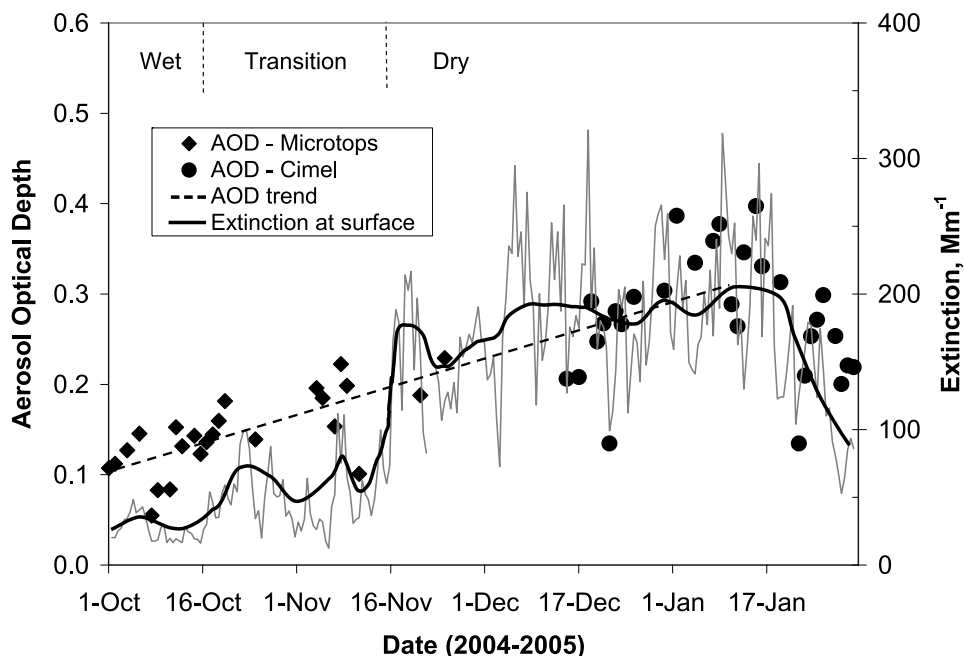


**Figure 11.** Aerosol optical depth (AOD) and measured extinction at 500 nm during the monsoon transition. Trend for Microtops AOD measurements is shown as dashed line.

continent and the air mass had just taken an indirect path to the observatory.

[40] As illustrated earlier in Figure 3b, higher altitudes received pollution from the mainland at an earlier date than the surface level. This phenomenon was also detected by aerosol optical depth (AOD) and lidar measurements [Ramana and Ramanathan, 2006]. At MCOH, the AOD at 500 nm was initially measured directly by a Microtops II handheld Sun photometer and later by a newly installed Aeronet CIMEL Sun photometer. The data was screened to remove periods when clouds affected the measurements. As a result, the blank spaces in the AOD measurements correspond to rainy or cloudy conditions. Low AOD values among larger values can usually be disregarded since they typically resulted from the clean period after rain events. The AOD average values  $\pm$  standard deviation for the wet, transitional, and dry monsoon period were  $0.12 \pm 0.03$ ,  $0.16 \pm 0.04$  and  $0.27 \pm 0.07$ , respectively. Figure 11 shows AOD measurements at 500 nm taken at the observatory along with the total aerosol extinction coefficient at 500 nm. The aerosol extinction was calculated from 550 nm data by adding the scattering and absorption coefficients together and then correcting to 500 nm using the ratio 550/500, which assumes an angstrom exponent of unity. The surface aerosol extinction average values  $\pm$  standard deviation for the wet, transitional, and dry monsoon period were  $30.1 \pm 9.2$ ,  $49.0 \pm 23.0$  and  $171.6 \pm 55.9 \text{ Mm}^{-1}$ , respectively. Being the additive result of absorption and scattering, the extinction coefficient shows the same rapid increase during November as seen in Figure 8, yet the AOD measurements, which reflect the aerosol optical properties for the total vertical column of the atmosphere, demonstrate a consistent and gradual increase over time starting in early October and suggests that pollution was progressively building up at the higher altitudes. The dashed line in Figure 11 is the trend line for the Microtops AOD

measurements and illustrates the gradual increase of extinction in the vertical column of air above the observatory. It was not until 15 November that polluted air originating from the mainland became persistent at the surface level in the Maldives. The abrupt change at the surface, with respect to the vertical column, is clearly visible in the smoothed extinction line of Figure 11.

[41] Since the absorption increased to a greater degree than the scattering with the arrival of the continental pollution (as seen in Figure 8), a darkening of the aerosol was observed. The coalbedo is defined as the fraction of total solar radiation loss attributed to absorption. The coalbedo is related to the single scatter albedo, or SSA, by the relationship  $(1 - \text{SSA})$ . The coalbedo was calculated from the aerosol absorption and scattering data (see Figure 8) using the following formula

$$\text{Coalbedo} = \frac{\sigma_a}{\sigma_s + \sigma_a} \quad (1)$$

where  $\sigma_s$  is the aerosol scattering coefficient and  $\sigma_a$  is the aerosol absorption coefficient. The time series for the coalbedo at 550 nm is shown in Figure 12 and shows that a distinct step increase in the average coalbedo occurred after 15 November. The error bars, given for only 1 out of every 8 points for readability, represent the uncertainty originating from the instrument errors propagated through the correction and data reduction procedures. The instrumental errors ranged from 10% to 40% depending upon the magnitude of the aerosol absorption and scattering. The error bars do not include natural variability in the aerosol over the 12 hour time period or other possible errors discussed in section 3.1. The coalbedo exhibited an average of  $0.028 \pm 0.015$  (standard deviation of  $1\sigma$ ) in early October. This value was most likely attributed to the lack of combustion pollution and the relative abundance of efficient scattering particles,

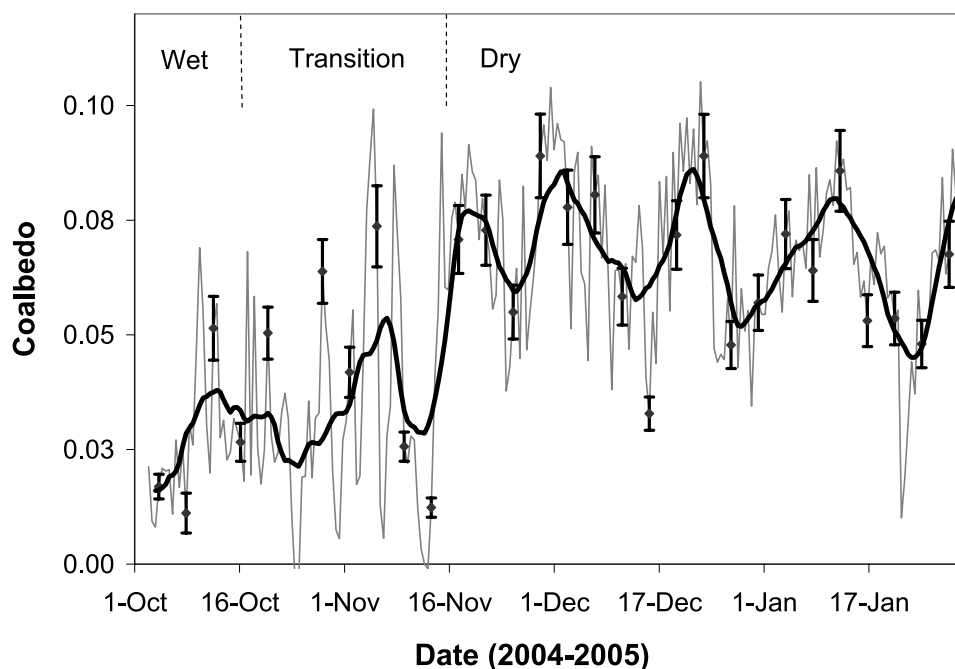


**Figure 12.** Coalbedo at 550 nm derived from aerosol optical properties during the monsoon transition at MCOH. The error bars represent propagation of instrument uncertainties through the data reduction techniques.

such as locally generated sea salt particles. With the dry monsoon, the coalbedo increased to an average of  $0.07 \pm 0.02$ , roughly a 2.5 fold increase from the wet monsoon season. These values are much lower than the 0.20–0.30 coalbedo values measured by *Eldering et al.* [2002] during INDOEX on the nearby island of Kaashidhoo. This discrepancy is likely explained by the INDOEX measurements being performed only on the submicron component of the aerosol and at a dry relative humidity. Because of the presence of highly scattering supermicron particles (as seen with the APS), the fractional absorption of the aerosol during APMEX was significantly lower relative to the INDOEX measurements. Moreover, the high ambient relative humidity promoted the uptake of water by the aerosol particles which resulted in much higher increase in scattering values as opposed to absorption values. With an increase in altitude above the site, the coalbedo would likely increase due to the reduced supermicron particle concentration and the lower relative humidity. A  $1 \mu\text{m}$  size cut alternating with the standard PM10 aerosol prior to the aerosol entering the nephelometer [see *Anderson and Ogren*, 1998] would be helpful for future experiments. The variability in the coalbedo prior to 15 November was due to the combination of local aerosol interferences, noise associated with minimum detection limits, and the sporadic arrival of high-altitude contaminated air from Asia. Variability still existed in the coalbedo values after the transition, but was more narrowly confined.

### 3.4. Black Carbon Measurements

[42] Black carbon was directly observed at MCOH using two distinct methods that employed optical and thermal methods. The aethalometer measured the light absorption of aerosol particles collected on a filter to arrive at BC mass concentrations. An interim value for light absorption was

generated using the method described by *Arnott et al.* [2005] and then converted to BC mass concentration ( $\text{g/m}^3$ ) by applying an absorption cross section value ( $\text{m}^2/\text{g}$ ), ACS, to the absorption coefficient ( $\text{m}^{-1}$ ). The ACS for ambient BC has been estimated to cover a wide range of values ( $5\text{--}20 \text{ m}^2/\text{g}$ ) depending upon location and sources of BC [*Liousse et al.*, 1993]. Typical average values for in situ BC aerosols fall in the range of  $7\text{--}10 \text{ m}^2/\text{g}$  [*Schnaiter et al.*, 2003; *Marley et al.*, 2001], but these methods usually did not address the interferences associated with scattering and filter loading. A second method for measuring BC involved collecting the aerosol onto quartz fiber filters and then using chemical techniques. The filter collection method determined elemental carbon (EC) by burning the collected particulate matter and detecting the evolved carbon. The method converted the resulting  $\text{CO}_2$  gas from combustion of the filter to methane and then used and FID (flame ionization detector) to quantify the amount of carbon [*Schauer et al.*, 2003]. (Henceforth BC will be used to indicate both EC and BC.) The isolation of the BC fraction from the organic fraction was accomplished by a combination of temperature limits, carrier gas, and light absorption markers detected during the analysis process.

[43] Figure 13 shows the agreement between the two methods of measuring BC at MCOH during the APMEX period. The trends and magnitudes for the filter and aethalometer method matched very closely. Both methods revealed a large increase in the average BC concentration on 15 November that is consistent with the increase in aerosol loading seen with both the physical and optical measurements. Figure 13 only extends until 2 December due to limitation in available filter data. The remaining BC data through 31 January 2005 follows the identical pattern as the absorption data in Figure 8 since the BC is calculated from the absorption coefficient using the simple

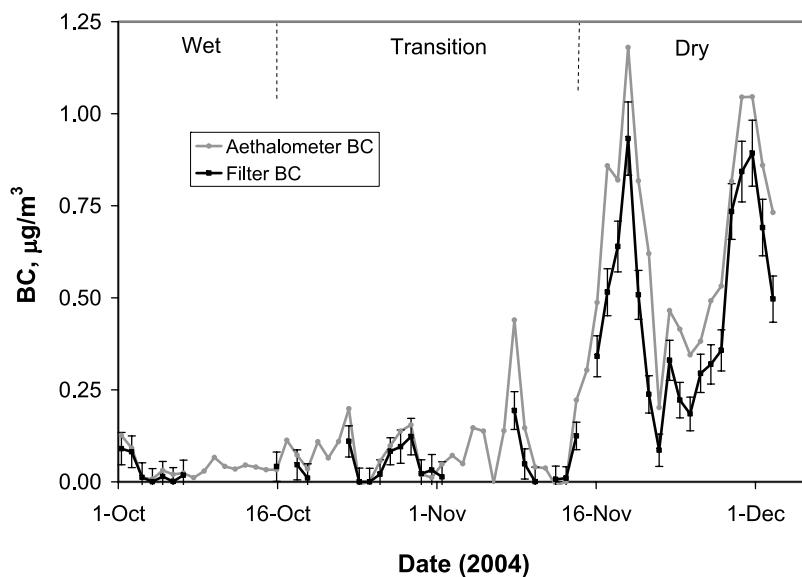


**Figure 13.** Black carbon mass concentration during the monsoon transition derived from both filter and aethalometer measurements.

proportional constant of  $10 \text{ m}^2/\text{g}$ . Error bars are shown for the filter data but are omitted for the aethalometer data to avoid overlap of error bars. The errors associated with the aethalometer method due to instrumental uncertainties range from 50% at  $0.05 \text{ } \mu\text{g}/\text{m}^3$  to 6% at  $1 \text{ } \mu\text{g}/\text{m}^3$ . These uncertainties do not include the other sources of error outlined in section 3.1.

[44] The correlation between the aethalometer measurements and the filter measurements is shown in Figure 14. The aethalometer data was initially assigned an ACS of  $10 \text{ m}^2/\text{g}$  for this comparison since this value is often applied in the literature [Lioussé et al., 1993; Marley et al., 2001; Schnaiter et al., 2003]. This value resulted in a slight offset between the aethalometer BC and filter BC which was

reflected in the slope of  $1.26 \pm 0.09$ . By using an ACS of  $12.6 \text{ m}^2/\text{g}$ , the aethalometer measurements were made to closely match with the filter measurements (slope = 1.0). Given the uncertainty of the correction method employed on the aethalometer data and the uncertainties associated with filter methods, the ratio of 1.26 in derived BC concentrations versus filter measurements validates the correction method.

[45] Table 3 presents the BC mass concentrations obtained from both the filter and aethalometer measurements. The aethalometer derived BC concentrations are given for both ACS values of 10 and  $12.6 \text{ m}^2/\text{g}$ . In general, using an ACS value of 10 would be customary unless

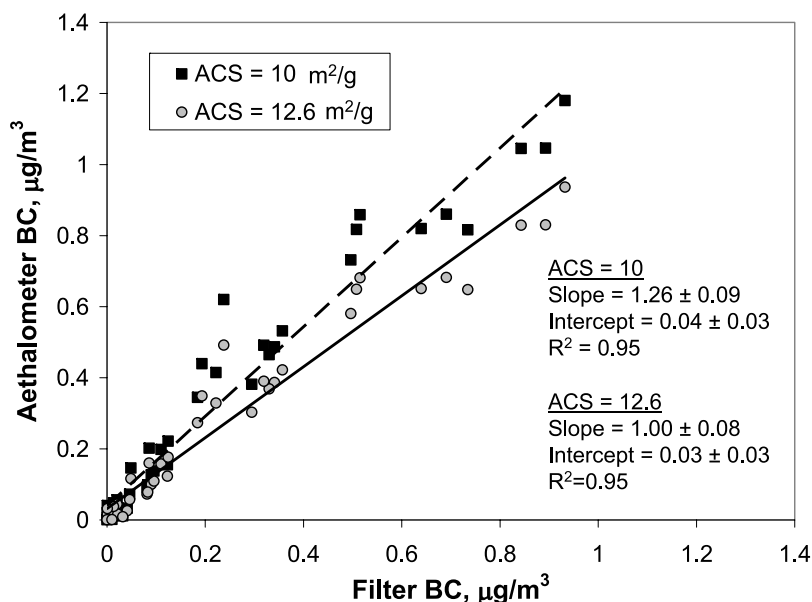


**Figure 14.** A comparison of filter and aethalometer based measurement methods for determining BC mass concentration. Each regression line represents a different absorption cross section (ACS) applied to the aethalometer data.

**Table 3.** Black Carbon Mass Concentrations During the Premonsoon, Transitional, and Postmonsoon Periods as Measured by Collected Filters and the Aethalometer<sup>a</sup>

Monsoon Period	Filter Mean $\pm$ SD, $\mu\text{g}/\text{m}^3$	Aethalometer Mean $\pm$ SD, $\mu\text{g}/\text{m}^3$	
		10 $\text{m}^2/\text{g}$	12.6 $\text{m}^2/\text{g}$
Wet	0.031 $\pm$ 0.038	0.041 $\pm$ 0.034	0.032 $\pm$ 0.027
Transitional	0.052 $\pm$ 0.055	0.072 $\pm$ 0.064	0.058 $\pm$ 0.051
Dry (truncated/filters)	0.48 $\pm$ 0.26	0.63 $\pm$ 0.32	0.50 $\pm$ 0.25
Dry (all data)	–	0.74 $\pm$ 0.30	0.59 $\pm$ 0.24

<sup>a</sup>The aethalometer data are presented for two different values of the absorption cross section.

calibrated agreement with filter results is desired. The occurrence of the higher ACS of 12.6  $\text{m}^2/\text{g}$  may not have a significant implication since it is likely an artifact arising from the uncertainties in the filter measurements [Currie *et al.*, 2002] and the aethalometer correction methods. To assist in a true comparison, the aethalometer data for the dry season is presented twice. One value is for the entire data set through 31 January 2005 and the other value is truncated at 2 December 2004 so as to correspond with the collection period of the filters. As seen in Figure 13, the results in Table 3 show that the BC mass concentrations increased by an order of magnitude with the arrival of the dry monsoon.

#### 4. Summary

[46] Measurements performed in the Republic of the Maldives in the Indian Ocean illustrated the distinct change in aerosol properties between the two South Asian monsoon seasons. During the wet monsoon, which runs from May to October, clean air was transported from the Southern Hemisphere. Consequently, the aerosol concentration was low and was dominated by supermicron particles. Under these pristine conditions and the transition period prior to the onset of the dry monsoon, the total aerosol concentration averaged  $770 \pm 440$  particles/ $\text{cm}^3$ . The scattering and absorption coefficients averaged  $28.8 \pm 10.8$  and  $0.87 \pm 0.56$   $\text{Mm}^{-1}$  during the wet monsoon. The coalbedo under these pristine conditions was very low with an average of  $0.028 \pm 0.015$ . The BC mass concentration during the wet monsoon as measured using an aethalometer was  $0.041 \pm 0.034$   $\mu\text{g}/\text{m}^3$ . Filter measurements of BC concentration gave a similar value of  $0.031 \pm 0.038$   $\mu\text{g}/\text{m}^3$ .

[47] After a 1 month transitional period, the dry monsoon arrived on 15 November 2004 as the wind shifted to the opposite direction and exposed the observatory to air from the Asian continent. An increase in aerosol concentration, especially accumulation mode particles, was observed. The average total particle concentration increased three fold to  $2100 \pm 560$  particles/ $\text{cm}^3$ . Similarly, the scattering and absorption increased to  $161 \pm 53$  and  $11.7 \pm 4.6$   $\text{Mm}^{-1}$ , respectively. This represented an increase by a factor of 5.6 and 13.5 as compared to the wet monsoon prior to 15 October. The most significant increase was in absorbing aerosols, which resulted in an increase of coalbedo by a factor of 2.5 to  $0.07 \pm 0.02$ . The BC mass concentration measured by two separate methods showed a magnitude increase with the arrival of the dry monsoon. The BC mass concentration measured by the filter method during the first two weeks of the dry monsoon was  $0.48 \pm 0.26$   $\mu\text{g}/\text{m}^3$ . The aethalometer derived BC mass concentration averaged  $0.74 \pm 0.30$   $\mu\text{g}/\text{m}^3$  for the first half (11 weeks) of the dry season of 2004–2005.

These results suggest a significant enhancement in the aerosol radiative forcing over the region as a consequence of the dry monsoon.

[48] **Acknowledgments.** This research was supported by NOAA under the grant NOAA/NA17RJ1231. Permission and assistance for use of observatory was provided by the Ministry of Environment and Construction, Government of Maldives, and the Department of Meteorology, Government of Maldives. Some AOD data were provided by the AERONET program of NASA. NCEP reanalysis data were provided by the NOAA CIRES Climate Diagnostics Center, Boulder, Colorado, USA, from their Web site at <http://www.cdc.noaa.gov/>. Hypsplit wind back trajectories were obtained using the HYSPLIT model of the NOAA ARL group (<http://www.arl.noaa.gov/ready/hysplit4.html>).

#### References

- Allen, G. A., J. Lawrence, and P. Outtakes (1999), Field validation of a semi-continuous method for aerosol black carbon (aethalometer) and temporal patterns of summertime hourly black carbon measurements in southwestern PA, *Atmos. Environ.*, **33**, 817–823.
- Anderson, T. L., and J. A. Ogren (1998), Determining aerosol radiative properties using the TSI 3563 integrating nephelometer, *Aerosol Sci. Technol.*, **29**(1), 57–69.
- Arnott, W. P., K. Hamasha, H. Moosmuller, P. J. Sheridan, and J. A. Ogren (2005), Towards aerosol light-absorption measurements with a 7-wavelength aethalometer: Evaluation with a photoacoustic instrument and 3-wavelength nephelometer, *Aerosol Sci. Technol.*, **39**(1), 17–29.
- Baron, P. A., and K. Willeke (Eds.) (2001), *Aerosol Measurement: Principles, Techniques, and Applications*, 2nd ed., John Wiley, Hoboken, N. J.
- Bond, T. C., T. L. Anderson, and D. Campbell (1999), Calibration and intercomparison of filter-based measurements of visible light absorption by aerosols, *Aerosol Sci. Technol.*, **30**(6), 582–600.
- Chowdhury, Z., L. S. Hughes, L. G. Salmon, and G. R. Cass (2001), Atmospheric particle size and composition measurements to support light extinction calculations over the Indian Ocean, *J. Geophys. Res.*, **106**(D22), 28,597–28,605.
- Chung, C. E., V. Ramanathan, and J. T. Kiehl (2002), Effects of the south Asian absorbing haze on the northeast monsoon and surface-air heat exchange, *J. Clim.*, **15**(17), 2462–2476.
- Currie, L. A., et al. (2002), A critical evaluation of interlaboratory data on total, elemental, and isotopic carbon in the carbonaceous particle reference material, NIST SRM 1649a, *J. Res. Natl. Inst. Stand. Technol.*, **107**(3), 279–298.
- Draxler, R. R., and G. D. Hess (1998), An overview of the HYSPLIT 4 modeling system for trajectories, dispersion, and deposition, *Aust. Meteorol. Mag.*, **47**, 295–308.
- Eldering, A., J. A. Ogren, Z. Chowdhury, L. S. Hughes, and G. R. Cass (2002), Aerosol optical properties during INDOEX based on measured aerosol particle size and composition, *J. Geophys. Res.*, **107**(D22), 8001, doi:10.1029/2001JD001572.
- Holton, J. R. (1992), *An Introduction to Dynamic Meteorology*, 3rd ed., 379 pp., Elsevier, New York.
- Intergovernmental Panel on Climate Change (IPCC) (2001), *Climate Change 2001: The Scientific Basis*, edited by J. T. Houghton et al., Cambridge Univ. Press, New York.
- Jacobson, M. Z. (2002), Control of fossil-fuel particulate black carbon and organic matter, possibly the most effective method of slowing global warming, *J. Geophys. Res.*, **107**(D19), 4410, doi:10.1029/2001JD001376.
- Kirchstetter, T. W., T. Novakov, and P. V. Hobbs (2004), Evidence that the spectral dependence of light absorption by aerosols is affected by organic carbon, *J. Geophys. Res.*, **109**, D21208, doi:10.1029/2004JD004999.
- Krishnamurti, T. N., B. Jha, J. Prospero, A. Jayaraman, and V. Ramanathan (1998), Aerosol and pollutant transport and their impact on radiative

- forcing over the tropical Indian Ocean during the January–February 1996 pre-INDOEX cruise, *Tellus, Ser. B.*, 50(5), 521–542.
- Lioussé, C., H. Cashier, and S. G. Jennings (1993), Optical and thermal measurements of black carbon aerosol content in different environments: Variation of the specific attenuation cross-section, sigma, *Atmos. Environ., Part A*, 27(8), 1203–1211.
- Marley, N. A., J. S. Gaffney, C. Baird, C. A. Blazer, P. J. Drayton, and J. E. Frederick (2001), An empirical method for the determination of the complex refractive index of size-fractionated atmospheric aerosols for radiative transfer calculations, *Aerosol Sci. Technol.*, 34(6), 535–549.
- Menon, S., J. Hansen, L. Nazarenko, and Y. F. Luo (2002), Climate effects of black carbon aerosols in China and India, *Science*, 297(5590), 2250–2253.
- Moorthy, K. K., S. S. Babu, and S. K. Satheesh (2005), Aerosol characteristics and radiative impacts over the Arabian Sea during the intermonsoon season: Results from ARMEX field campaign, *J. Atmos. Sci.*, 62(1), 192–206.
- Ramana, M. V., and V. Ramanathan (2006), Abrupt transition from natural to anthropogenic aerosol radiative forcing: Observations at the ABC-Maldives Climate Observatory, *J. Geophys. Res.*, doi:10.1029/2006JD007063, in press.
- Ramanathan, V., and P. J. Crutzen (2003), New directions: Atmospheric brown “clouds,” *Atmos. Environ.*, 37(28), 4033–4035.
- Ramanathan, V., et al. (2001), Indian Ocean Experiment: An integrated analysis of the climate forcing and effects of the great Indo-Asian haze, *J. Geophys. Res.*, 106(D22), 28,371–28,398.
- Ramanathan, V., C. Chung, D. Kim, T. Bettge, L. Buja, J. T. Kiehl, W. M. Washington, Q. Fu, D. R. Sikka, and M. Wild (2005), Atmospheric brown clouds: Impacts on south Asian climate and hydrological cycle, *Proc. Natl. Acad. Sci. U. S. A.*, 102(15), 5326–5333.
- Schauer, J. J., et al. (2003), ACE-Asia intercomparison of a thermal-optical method for the determination of particle-phase organic and elemental carbon, *Environ. Sci. Technol.*, 37(5), 993–1001.
- Schnaiter, M., H. Horvath, O. Mohler, K. H. Naumann, H. Saathoff, and O. W. Schöck (2003), UV-VIS-NIR spectral optical properties of soot and soot-containing aerosols, *J. Aerosol Sci.*, 34(10), 1421–1444.
- Sheridan, P. J., et al. (2005), The Reno Aerosol Optics Study: An evaluation of aerosol absorption measurement methods, *Aerosol Sci. Technol.*, 39, 1–16.
- Verver, G. H. L., D. R. Sikka, J. M. Lobert, G. Stossmeister, and M. Zachariasse (2001), Overview of the meteorological conditions and atmospheric transport processes during INDOEX 1999, *J. Geophys. Res.*, 106(D22), 28,399–28,413.

---

C. E. Corrigan and V. Ramanathan, Scripps Institution of Oceanography, 9500 Gilman Drive, La Jolla, CA 92037, USA. (ccorrigan@ucsd.edu)

J. J. Schauer, Department of Civil and Environmental Engineering, University of Wisconsin-Madison, 148 Water Science and Engineering Laboratory, 660 North Park Street, Madison, WI 53706-1484, USA.